

Determination of 1929 Asteroid Rotation Periods from WISE Data

ADRIAN L.H. LAM,^{1,2} JEAN-LUC MARGOT,^{3,1} EMILY WHITTAKER,³ AND NATHAN MYHRVOLD⁴

¹*Department of Physics and Astronomy, University of California, Los Angeles, CA 90095, USA*

²*Department of Electrical Engineering, University of California, Los Angeles, CA 90095, USA*

³*Department of Earth, Planetary, and Space Sciences, University of California, Los Angeles, CA 90095, USA*

⁴*Intellectual Ventures, 3150 139th Ave SE, Bellevue, WA 98005, USA*

ABSTRACT

We used 22 μm (W4) Wide-field Infrared Survey Explorer (WISE) observations of 4420 asteroids to analyze lightcurves and determined spin period estimates for 1929 asteroids. We fit second-order Fourier models at a large number of trial frequencies to the W4 data and analyzed the resulting periodograms. We initially excluded rotational frequencies exceeding 7.57 rotations per day ($P < 3.17$ hr), which are not sampled adequately by WISE, and periods that exceed twice the WISE observation interval, which is typically 36 hr. We found that three solutions accurately capture the vast majority of the rotational frequencies in our sample: the best-fit frequency and its mirrors around 3.78 and 7.57 rotations per day. By comparing our solutions to a high-quality control group of 752 asteroid spin periods, we found that one of our solutions is accurate (within 5%) in 88% of the cases. The best-fit, secondary, and tertiary solutions are accurate in 55%, 27%, and 6% of the cases, respectively. We also observed that suppression of aliased solutions was more effective with non-uniform sampling than with quasi-uniform sampling.

1. INTRODUCTION

The rotational period of an asteroid is a physical property that is important in a wide range of planetary science and space exploration contexts. A rotational period measurement is essential to the characterization of the rotational state (e.g., [Pravec et al. 2002](#)), which informs our understanding of an asteroid’s interior and morphology (e.g., [Scheeres et al. 2015](#)), dynamical evolution through the Yarkovsky and YORP effects (e.g., [Vokrouhlický et al. 2015](#); [Greenberg et al. 2020](#)), and the formation and evolution of binaries, triples, and pairs (e.g., [Margot et al. 2015](#); [Walsh & Jacobson 2015](#)). Spin rate distributions place bounds on the dynamical and collisional evolutions of the main belt of asteroids (e.g., [Bottke et al. 2015](#)), and therefore the characteristics of the near-Earth asteroid population, which governs the history of impact cratering in the inner solar system and affects planetary defense efforts. Spin periods also provide useful initial conditions when modeling the shape (e.g., [Ostro et al. 2002](#); [Benner et al. 2015](#); [Durech et al. 2015](#)) and thermophysical properties (e.g., [Delbo et al. 2015](#)) of asteroids. In these contexts, the availability of a small number of candidate spin periods is extremely valuable. One can test the model with each trial period and promptly identify the correct period. This fact motivated in part our inclusion of secondary spin period solutions in our results, in addition to our primary, best-fit period solutions.

Several approaches have been used to measure the rotational periods of asteroids with high precision, including Earth-based (e.g., [Pravec et al. 2002](#)) or space-based (e.g., [Hora et al. 2018](#)) photometric observations or a combination of the two (e.g., [Durech et al. 2018](#)), as well as Earth-based radar observations (e.g., [Ostro et al. 2006](#); [Naidu et al. 2015](#)). Optical lightcurve photometry based on wideband measurements of the sunlight reflected by the asteroid is the most common approach. Here we use infrared lightcurves to determine asteroid spin periods.

During its six-month primary mission, the WISE spacecraft ([Wright et al. 2010](#)) conducted a whole-sky infrared survey at four infrared bands (W1–4) centered at 3.4, 4.6, 12, and 22 μm . All four detectors were simultaneously exposed, producing up to four independent photometric measurements ([WISE Team 2020](#)). The high-quality, multi-band IR observations of $\sim 100,000$ asteroids have been used to estimate asteroid diameters and albedos (e.g., [Mainzer](#)

et al. 2015). Improved algorithms applied to a curated set of thousands of asteroids yielded refined estimates as well as estimates for asteroids not previously analyzed (Myhrvold et al. 2022).

Both the cadence and length of an asteroid lightcurve observing campaign determine the parameters that can be reliably recovered from the observations. Durations on the order of days/months/years, such as survey data from the Palomar Transient Factory (PTF) (Waszczak et al. 2015), provide an opportunity to sample the object at different phase angles and to recover parameters of the phase function (Muinonen et al. 2010). Densely sampled observations that span at least a complete rotational cycle provide the best opportunity to determine the spin period. WISE observations of asteroids present a challenge for lightcurve analyses because they take place over short intervals with sparse cadence, typically yielding only ~ 16 observations over a ~ 36 -hour interval (Wright et al. 2010). Nevertheless, most asteroids experience a few rotations in 36 hr, such that WISE data can in principle be used to estimate the spin periods of thousands of asteroids (Cutri et al. 2019).

Đurech et al. (2015) combined sparse photometry, including WISE data, to derive the spin period of one asteroid. Hanuš et al. (2015) combined WISE thermal infrared data and other data to obtain shape models and spin periods of six asteroids. Their work has since been expanded to derive 1451 spin periods for asteroids observed by WISE (Đurech et al. 2018). Here, we use the well-curated data set from the fully cryogenic phase of the WISE mission (Myhrvold et al. 2022; Margot et al. 2023) to estimate spin periods for hundreds of asteroids.

The Lightcurve Database (LCDB) (Warner, B.D. and Harris, A.W. and Pravec, P. 2021) is a compilation of most known lightcurve measurements from various sources. Each lightcurve is assigned a quality code between 0 (incorrect) and 3 (best) by the database curators to convey the confidence level in the uniqueness and accuracy of the rotational period estimate. We used the LCDB to evaluate the reliability of our solutions and to train a machine learning reliability classifier.

2. METHODS

2.1. Overview

Our methods closely follow those of Waszczak et al. (2015), who used sparse photometry from the Palomar Transient Factory (PTF) to determine $\sim 9,000$ reliable asteroid spin periods. Their method is conceptually straightforward. For each trial period, one fits a Fourier series model (Harris et al. 1989, Equation 1) to the observed flux values and computes the sum of squares of the flux residuals. The Fourier series is truncated after the second harmonic, a simplification that rests on the assumption that the object is approximately ellipsoidal in shape. It is also consistent with the fact that the second harmonic dominates asteroid lightcurves with amplitudes greater than 0.4 magnitudes (Harris et al. 2014). Although this model is insufficient to capture the full details of the lightcurve, it is adequate to recover the spin period in most instances, as can be verified by comparing the solutions to high-quality (quality code 3- or above) solutions published in the lightcurve database (LCDB) (Warner, B.D. and Harris, A.W. and Pravec, P. 2021). A similar method was also used by Chang et al. (2017) to determine 2780 reliable asteroid rotation periods from the PTF.

Waszczak et al. (2015)'s method is directly applicable to WISE photometry, which typically contains at least ~ 16 observations of each asteroid with a nominal 1.59 hr cadence over a ~ 36 hr period. Although this observational mode prevents the determination of spin periods for fast ($P < 3.17$ hr) and slow ($P > 72$ hr) rotators, most asteroids have spin periods that are amenable to characterization with this technique. Based on reliable LCDB statistics (quality code 3- or higher) and the range of diameters (0.28–72.2 km) in the Myhrvold et al. (2022) sample, we estimate that fewer than 17% of asteroids in our sample have a spin period smaller than 3.17 hr.

Waszczak et al. (2015) were able to fit for a photometric phase function because their observations were obtained over a wide range of phase angles. In contrast, WISE observations typically span a narrow range of phase angles and we did not attempt to evaluate the phase function. Phase angles remained nearly constant during the short observation intervals, and phase angle effects were absorbed by the zeroth-order coefficient of the Fourier series, i.e., mean magnitude.

We compared our method to results obtained with the more traditional Lomb-Scargle periodogram (Press et al. 1992) (Sections 2.9 and 3.2).

2.2. Data Set

2.2.1. Initial Data Set

We used the carefully curated data set of Myhrvold et al. (2022), who eliminated measurements with artifacts, low signal-to-noise ratio (S/N), poor photometric quality, saturation, questionable PSF fits, background confusion, problematic near-conjunction conditions, or large discrepancies between ephemeris predictions and reported position. Their data set provides high-quality flux measurements in all four infrared bands for 4420 asteroids. For a small fraction (6%, 265 asteroids), WISE observations were obtained in distinct (almost always two) epoch clusters separated by more than 30 days. We determined independent solutions for each cluster of observations because they were obtained at different phase angles. Although our analysis is done on individual clusters, we may refer to the clusters as asteroids for ease of presentation.

2.2.2. Assignment of Flux Uncertainties

Both Hanuš et al. (2015) and Myhrvold (2018) have shown that uncertainties reported by the WISE pipeline underestimate actual flux uncertainties. Hanuš et al. (2015) used ~ 400 pairs of asteroid detections observed in quick succession (~ 11 s) to quantify actual flux uncertainties in W3 and W4. They found that uncertainties reported in the WISE database underestimate actual uncertainties by factors 1.4 and 1.3 in W3 and W4, respectively. Myhrvold (2018) expanded this analysis to bands W1–W4 and included a much larger number of pairs (7834, 11202, 125318, and 59049 in W1–W4, respectively). Here, we further expanded the number of pairs and fit Gaussians to the distributions of Z values ($Z = (f_1 - f_2)/\sqrt{\sigma_1^2 + \sigma_2^2}$) (Myhrvold 2018, Equation 3) after removing $\sim 1\%$ of pairs with $|Z| > 5$. The elimination is required because the tails of the distributions are non-Gaussian even though the cores of the distributions are well approximated by Gaussians. We list the correction factors in all four bands for completeness (Table 1). We assigned uncertainties to the flux measurements by multiplying the uncertainties reported in the WISE database with the relevant correction factor.

Band	Number of pairs	Correction factor	Median σ (corrected)
W1	29936	1.224	0.195
W2	34462	1.120	0.132
W3	170232	1.479	0.035
W4	120225	1.218	0.058

Table 1. Correction factors that are required to convert flux uncertainties reported in the WISE pipeline to actual uncertainties. The second column shows the number of remaining pairs after elimination of $\sim 1\%$ of pairs with uncharacteristically large flux differences. The last column shows the median flux uncertainties in magnitude units after correction.

2.2.3. Band Selection

We focus on observations in W4 for two reasons. First, thermal emission from asteroids is stronger, S/N is higher, and the number of observations in the curated data set is higher in W3 and W4 than in W1 and W2. Second, the observation cadence of the original and curated WISE data is generally non-uniform, with time intervals as small as 11 s, a most common time interval of 1.59 hr, a frequent time interval of 2×1.59 hr = 3.17 hr, and occasional time intervals at higher multiples of 1.59 hr. W4 observations provide the best observational cadence, whereas W3 observations have a higher fraction of asteroids with a longer cadence (Figure 1), which increases the susceptibility to aliasing difficulties (Section 2.4).

We are not concerned with thermal lags or differences in lightcurve amplitudes compared to optical lightcurves, as they are inconsequential to the determination of spin periods. In addition, Āurech et al. (2018) demonstrated that thermal lightcurves in W3 and W4 are qualitatively consistent with optical lightcurves.

While multiband lightcurve fits could in principle be envisioned, their utility in the context of spin period determinations with WISE data is limited because the exposures in the four bands are simultaneous, such that they sample roughly the same rotational phase. The determination of phase lags among observations in the four WISE bands is potentially informative but beyond the scope of the current work.

2.2.4. Data Selection Filters

We applied several preprocessing filters in order to identify lightcurves most suitable for rotational period determination. Each observation cluster must pass all of the following filters to qualify for analysis, otherwise it is discarded.

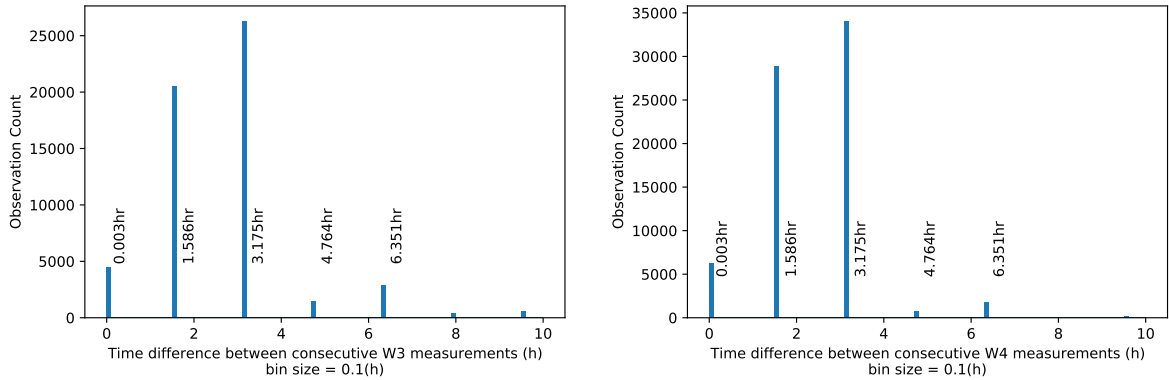


Figure 1. Histograms of W3 (left) and W4 (right) sampling intervals in the Myhrvold et al. (2022) data set.

First, we focus on lightcurves that have at least 12 data points in W4. Second, we eliminated lightcurves where the peak-to-peak variation in flux magnitude $W4_{\text{red}} < 0.3$ mag, where we used magnitudes reduced to the values that would be observed at an asteroid-sun distance $r_{\text{as}} = 1$ au and asteroid-observer distance $r_{\text{ao}} = 1$ au. This filter eliminates low-amplitude lightcurves, which may be ambiguous with respect to spin period determination (Harris et al. 2014). This filter effectively eliminates very slow rotators, which are not considered in our analysis anyway (Section 2.3). Third, we eliminated any lightcurve that does not have an adequate observation cadence. Specifically, we required at least one time interval between consecutive observations to fall in the range 1.55–1.58 h, which corresponds to the WISE spacecraft orbital period (Wright et al. 2010). Observation clusters that have a longer (3.10–3.16 h) minimum sampling interval are more susceptible to severe aliasing (Section 2.4) and are discarded.

The filtered data set contains a total of 3061 asteroids, with 3225 observation epochs and 57,532 W4 photometric measurements. In this data set, 164 (5.3%) out of the 3061 asteroids contain two observation clusters, and none have more than 2 observation clusters.

On average, an observation cluster contains 16 data points and spans 36 hr.

W4 flux observations	57,532
Median flux uncertainty	0.067
Median number of data points per cluster	16
Median observation span of clusters	1.522 days

Table 2. Characteristics of filtered data set

2.3. Fitting Procedure

An effective method for identifying periodicities in sparse data is a “period scan”, where a model lightcurve is fitted to the data for a range of trial spin periods and a measure of the misfit (i.e., fit dispersion) is evaluated at each trial period (Harris et al. 2012). The misfit metric is the usual sum of squares of residuals:

$$\chi^2 = \sum_{i=1}^N \frac{(O_i - C_i)^2}{\sigma_i^2}, \quad (1)$$

where O_i is the i -th observation, C_i is the i -th computed (modeled) value, σ_i is the uncertainty associated with the i -th observation, and the index i ranges from 1 to N , the total number of observations. The observations are the reduced flux magnitudes (Section 2.2.4), the uncertainties are the magnitude uncertainties from the WISE database multiplied by the relevant correction factors (Section 2.2.2), and the computed values are obtained by fitting a second-order Fourier model to the data similar to Waszczak et al. (2015)’s formulation. Specifically,

$$C_i = A_{0,0} + A_{1,1} \sin\left(\frac{2\pi}{P} t_i\right) + A_{2,1} \cos\left(\frac{2\pi}{P} t_i\right) + A_{1,2} \sin\left(\frac{4\pi}{P} t_i\right) + A_{2,2} \cos\left(\frac{4\pi}{P} t_i\right), \quad (2)$$

where t_i is the light-time corrected epoch of the i -th observation, P is the trial spin period, and the $A_{i,j}$ are the five adjustable Fourier coefficients.

We considered a range of evenly spaced rotational frequencies between $f = 0$ and 7.5662 rotations per day, where $f_{\max} = 7.5662$ rot/day ($P \simeq 3.17$ h) represents the fastest rotation that can be Nyquist sampled with the WISE observational cadence (Section 2.4). However, we showed that it is possible to recover the periods of fast rotators by taking advantage of the mirroring properties of aliased signals. We did not attempt to recover rotational frequencies that exceed 11 rotations per day, which correspond approximately to the rotational frequency at which centrifugal acceleration at the equator exceeds the acceleration due to self-gravity for typical asteroid densities, the so-called spin barrier at $P \simeq 2.2$ hr (Pravec et al. 2002). The overwhelming majority of asteroids detected by WISE and included in our data set are large and experience fewer than 11 rotations per day.

The least-squares minimizer is an ordinary linear least-squares solver that follows Waszczak et al. (2015, tar.gz file), except that we do not fit for phase curve parameters. We also computed the reduced chi-squared metric $\chi^2_\nu = \chi^2/(N-5)$, where the number of degrees of freedom $\nu = N-5$ represents the number of data points minus the number of free model parameters.

The discrete Fourier transform of a time series with duration T yields a frequency resolution of $1/T$. In this work, we chose to increase the frequency resolution by an oversampling factor of 10 in order to better resolve peaks in the period scan. The number of trial frequencies was therefore set to $10 \times T \times f_{\max}$.

We used an iterative procedure similar to Waszczak et al. (2015) where an increasingly large ‘‘cosmic error’’ is added to the observation uncertainties. The cosmic error is initialized as 0.002 mag in the first iteration and is multiplied by 1.5 in each subsequent iteration. The purpose of the cosmic error is to inflate the measurement uncertainties in order to reflect the model’s inability to accurately represent asteroid lightcurves with a Fourier series truncated at the second harmonic. The cosmic error does not affect the periodicities identified in the lightcurve, but it does affect the confidence intervals assigned to the period estimates.

We followed Waszczak et al. (2015) and Harris et al. (2014) in preferring double-peaked folded lightcurves. To identify the number of peaks in the lightcurve, we generated a synthetic folded lightcurve with the fitted Fourier coefficients and candidate period, sampled it with 10,000 points, and analyzed the samples with Matlab’s built-in function `find_peaks`¹. For each double-peaked solution, we computed the heights of each peak relative to the lightcurve’s global minimum.

There are two possible paths to convergence. At the end of each iteration, the solution with the lowest χ^2_ν is selected if and only if it satisfies three conditions: (1) the folded lightcurve is double-peaked; (2) the height of the highest peak is at least twice that of the lowest peak; and (3) $\chi^2_\nu < 3$. If conditions (1) or (2) are not satisfied, the solution at half-frequency is considered and is adopted if it satisfies the same three conditions. Otherwise, the cosmic error is increased and the next iteration begins. If the cosmic error reaches 0.1 mag, the fit is deemed unsuccessful.

2.4. Aliasing

The cadence of observations determines the sampling intervals between consecutive photometric measurements. The Nyquist sampling criterion requires that at least two samples of a periodic signal be obtained per cycle in order to identify the periodicity unambiguously. Apart from the fortuitous double detections obtained ~ 11 s apart (Section 2.2.2), the smallest sampling interval in WISE data is approximately 1.59 hr, which is dictated by WISE’s ~ 15 daily orbital revolutions (Wright et al. 2010). Asteroids sampled with the 1.59 hr cadence and rotation periods larger than 3.17 hr ($f < 7.5662$ rot/day) are usually Nyquist sampled, i.e., suffer no aliasing.

Assuming uniform sampling, the signatures of asteroids with rotation periods between 1.59 hr and 3.17 hr appear aliased in the period scan in a predictable manner, specifically:

$$f_{\text{alias}} = 2f_{\text{Nyq}} - f_{\text{spin}}, \quad (3)$$

where $f_{\text{Nyq}} = 7.5662$ rot/day is the critical Nyquist frequency or folding frequency, f_{spin} is the underlying true rotational frequency, and f_{alias} is the aliased frequency. For example, an asteroid rotating at the spin barrier of 2.2 h (10.9 rot/day) exhibits signatures at 2.2 h (10.9 rot/day) and 5.66 h (4.24 rot/day).

Absent additional information, a period scan may yield inconclusive results with respect to these two solutions. However, folding about the 7.5662 rot/day axis remains limited because only about 17% of asteroids in our sample

¹ <https://www.mathworks.com/help/signal/ref/findpeaks.html>

experience rotation rates that exceed 7.5662 rot/day (Section 2.1). The overwhelming majority of asteroids detected by WISE and included in our data set are large and experience fewer than 11 rotations per day.

It is frequent for the interval between consecutive W4 measurements to be 3.17 hr instead of the nominal cadence of 1.59 hr, e.g., when poor-quality flux measurements are eliminated. As a result, we also expected and observed (Section 3) folding of the periodogram about $f_{\text{Nyq}'} = 3.7831$ rot/day. The folded frequency happens to be correct in a substantial fraction of cases, which we used to our advantage as it is calculable and therefore recoverable with no loss of precision.

Additional aliasing considerations are described in Appendix A.

2.5. S/N Calculations

A period scan may return multiple peaks with low misfit values. S/N metrics are useful in determining whether a peak is likely to represent a genuine rotational signature as opposed to a noise artifact. We adopted two S/N metrics. One metric follows Waszczak et al. (2015) and quantifies the height of the peak with respect to the median misfit in terms of an estimation to the standard deviations of the misfit variations:

$$S/N_{\text{W}} = \frac{|\chi_{\text{min}}^2 - \chi_{\text{median}}^2|}{(\chi_{84\%}^2 - \chi_{16\%}^2)/2}, \quad (4)$$

where the denominator includes percentiles of the misfit distribution corresponding to ± 1 standard deviations from the median. The second metric follows Harris et al. (2012) and associates the misfit outside of minima, which we approximated by $\chi_{95\%}^2$, to the quadratic sum of the amplitude of lightcurve variation (a) and the noise in the data (n). It also associates the minimum misfit to the square of the single-point data scatter after removal of the signal (n^2), and assigns an overall noise level to the solution equal to $n/\sqrt{\nu} = n/\sqrt{(N-5)}$. We have

$$(a^2 + n^2) = \chi_{95\%}^2/N, \quad (5)$$

$$n^2 = \chi_{\text{min}}^2/N, \quad (6)$$

$$\text{signal} = a = \sqrt{(\chi_{95\%}^2 - \chi_{\text{min}}^2)/N} \quad (7)$$

$$\text{noise} = n' = \sqrt{\chi_{\text{min}}^2/N/\sqrt{(N-5)}} \quad (8)$$

$$S/N_{\text{H}} = a/n' = \sqrt{\frac{\chi_{95\%}^2 - \chi_{\text{min}}^2}{\chi_{\text{min}}^2}} \sqrt{(N-5)} \quad (9)$$

2.6. Assignment of Spin Period Uncertainties

Once the best-fit peak was identified, we assigned a 1σ uncertainty to the fitted period by computing the periods corresponding to a constant chi-square boundary (Press et al. 1992, Section 15.6). Specifically, we computed the periods at which $\chi^2 = \chi_{\text{min}}^2 + \Delta\chi^2(68.3\%, \nu = 5) = \chi_{\text{min}}^2 + 5.86$, where χ_{min}^2 is the minimum misfit.

2.7. Post-processing Filters

Because the duration and cadence of WISE observations are not optimal for the unambiguous determination of spin periods, it was important to remove solutions that are likely unreliable. We applied the following filters:

(1) Reject slow rotators. We required observations over at least 180 degrees of rotational phase and rejected any solution with a best-fit period that is two or more times longer than the data span.

(2) Reject anomalously high amplitude lightcurves. We eliminated solutions where the peak-to-peak amplitude of the fitted solution was three or more times larger than the peak-to-peak amplitude of the observations. The peak-to-peak amplitude of the lightcurve was determined numerically while evaluating the lightcurve with the best-fit Fourier coefficients.

(3) Reject low S/N solutions. Low S/N solutions are likely spurious and were eliminated. In practice, we found that the S/N formulation of Harris et al. (2012) was more effective than that of Waszczak et al. (2015), perhaps due in part to the relatively small number of (noisy) observations. Solutions were rejected when $(S/N)_{\text{H}} < 5$.

The solutions that passed all of the above filters are reported below. We have evidence that most of these solutions are accurate (Section 3), but we also expect a fraction of aliased or incorrect solutions in this set.

2.8. Machine Learning Reliability Classifier

Waszczak et al. (2015) pioneered the usage of a machine learning (ML) classifier to improve the reliability of asteroid lightcurve fits. They applied a random forest (RF) algorithm, which is a supervised machine learning algorithm that utilizes an ensemble of weak decision tree predictors to increase prediction power. The hypothesis underpinning a machine learning classifier is that certain appropriately chosen features associated with a lightcurve solution jointly carry non-trivial information regarding the reliability of the solution. Given a labeled training set that includes both the values of the features and a reliability indicator, an ML algorithm can be trained to detect relations within the feature space and predict a reliability indicator for lightcurve solutions that do not have a reliably known period (i.e., solutions that are not in the training set). A Random Forest classifier makes predictions via a majority voting process by its ensemble of decision trees. For each sample, the classifier generates a probability derived from the voting process, then makes a binary prediction (i.e., reliable or unreliable) on the basis of a user-defined probability threshold. Waszczak et al. (2015)’s classifier was trained with about 1000 lightcurves with known reference periods and improved the overall success rate from $\sim 66\%$ to $\sim 80\%$ for 19,000 lightcurves.

Because our work also involved the analysis of thousands of sparse lightcurve, we initially applied an RF algorithm in an attempt to identify the most reliable lightcurve solutions. The RF classifier was able to provide a modest improvement to the success rate of our primary solutions (from 55% to 70%), but it also marked correct solutions as incorrect. Because the recovery of spin periods among our three solutions was so high (88%) and the performance of the RF classifier was limited, we ultimately decided against providing a potentially flawed reliability indicator.

2.9. Lomb-Scargle Periodogram

The Lomb-Scargle (LS) periodogram (Lomb 1976; Scargle 1982) is a standard algorithm that enables the analysis of periodicities in unevenly sampled time series, such as asteroid lightcurves. We explored the performance of the LS periodogram as an alternative to our default pipeline. Our LS pipeline follows the implementation in standard libraries and does not include iterative adjustment of uncertainties, requirement for double-peaked solutions, and post-fit filters implemented in our default pipeline.

We used the generalized LS algorithm of Zechmeister & Kürster (2009) as implemented in the astropy package². This implementation takes observational uncertainties into account and enables the estimation of a floating mean. We deployed both first-order and second-order LS periodograms.

In the first-order LS implementation, we followed McNeill et al. (2019) and set the estimated rotational period at twice the best-fit LS period to conform to the double-peak nature of asteroid lightcurves. We admitted only solutions with a false-alarm probability (FAP) less than 10%.

The second-order LS implementation is similar to the periodogram calculation used in our default pipeline but does not include any post-fit filter.

3. RESULTS

3.1. Default pipeline

We present the period solutions that successfully converged in the Fourier fitting algorithm and passed the post-fit filters (Section 2.7). The period solutions of 2008 ($\sim 62\%$) out of the initial 3225 lightcurves fulfilled both inclusion criteria.

To test the reliability of our results, we compared our spin period estimates to high-quality (quality code 3- or higher) rotational periods published in the LCDB. We quantified the fraction of solutions that were within 5% of the LCDB solution, which are deemed to be accurate solutions. At the time of writing, there were 752 solutions (representing 702 unique asteroids) among our 2008 solutions with a suitable LCDB estimate. We refer to this set of solutions as the ‘LCDB reference group’.

In the LCDB reference group, the fitted period was found to be accurate (within 5%) in 55% of the cases. Notably, the relative errors of the fitted periods exhibit a bimodal distribution (Figure 2). The two modes bifurcate at a fractional error of approximately 5%, which provides a posteriori justification for selecting a 5% threshold for accuracy.

Our spin period solutions are listed in Table 3. Figure 3 illustrates an example of a favorable situation with a short (1.59 hr) cadence and relative long (6 days) duration, which yields a solution with high S/N and no aliasing. We found

² <https://docs.astropy.org/en/stable/timeseries/lombscargle.html>

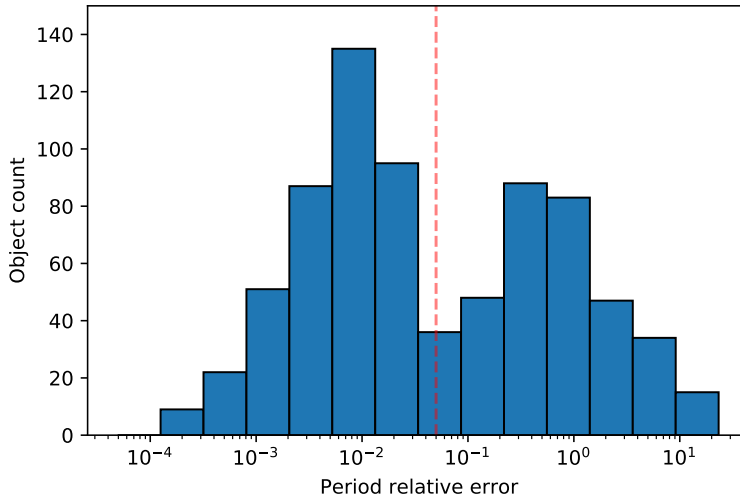


Figure 2. Histogram of fractional accuracy in spin period obtained by comparing our period solutions to the corresponding LCDB reference periods. The left and right clusters correspond to the accurate and inaccurate period estimates, respectively. The red line denotes the 5% accuracy threshold.

that it is possible to successfully recover the spin period even when the observation span is comparable to the spin period (Figure 4). Our analysis also identified correct spin periods in situations where the minimum χ^2 value is not markedly different from other competing solutions (Figure 5). When multiple periodogram peaks have comparable χ^2 values, the potential for an incorrect solution exists.

We validated our results by plotting our best-fit rotational frequencies against LCDB values for the LCDB reference group (Figure 6). In frequency space, which reveals folding behavior, the structure of the solutions is striking. Most of the inaccurate solutions are in fact aliases of the correct frequencies folded about the $f = 3.7831$ rot/day axis or, less frequently, the $f = 7.5662$ rot/day axis. Figures 7, 8, and 9 illustrate three examples.

For this reason, we list both the best-fit frequency and its mirror values in Table 3. One of these solutions is correct (within 5%) in 88% (659/752) of the cases in the LCDB reference group. We posit that the accuracy rate is similar for asteroids that are not in the LCDB reference group. The best-fit, secondary (mirrored about 3.7831 rot/day), and tertiary (mirrored about 7.5662 rot/day) solutions are accurate in 55%, 27%, and 6% of the cases, respectively.

Inaccurate solutions that are not mirrors of correct values are visible outside of the X pattern on Figure 6. Figure 10 illustrates a failed solution.

A number of solutions deemed to be inaccurate cluster near the accurate solutions along the blue diagonal, especially at low frequencies. This behavior indicates that our 5% criterion is a conservative metric of accuracy, and that additional solutions are in fact close to the correct value.

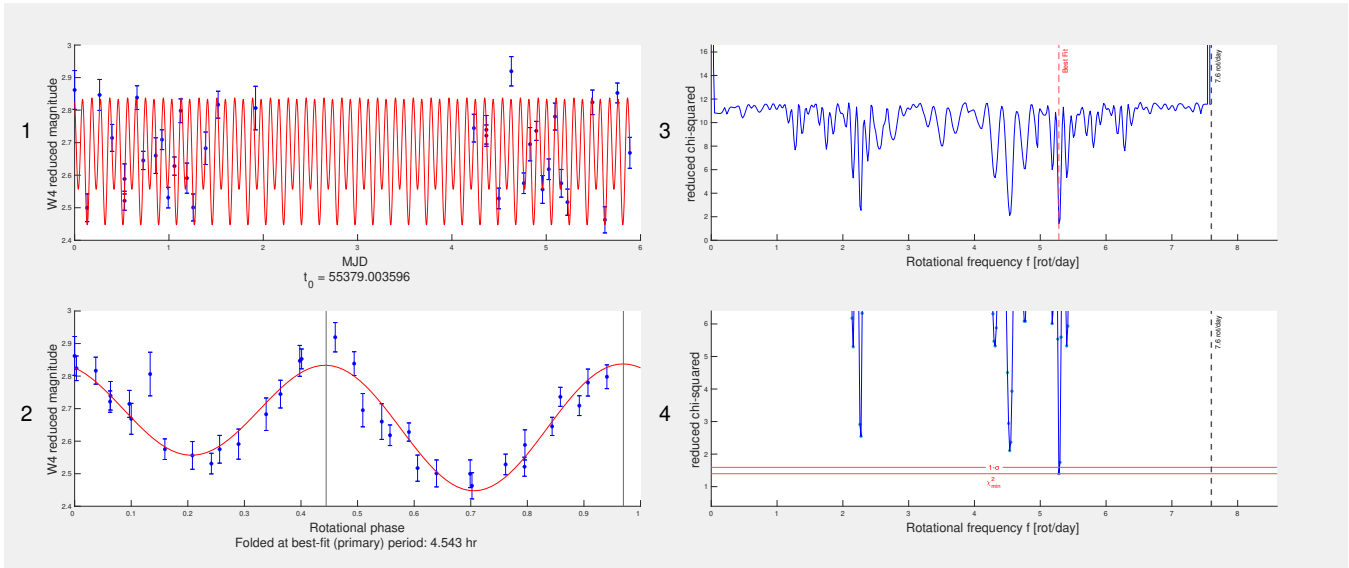


Figure 3. Spin period solution for asteroid 296 obtained from 35 W4 observations spanning 6 days. The period solution at 4.543 ± 0.014 hr is in good agreement with the LCDB value of 4.5385 hr. The data exhibit short (1.59 h) sampling intervals over a long observation span, and the periodogram is free of aliases.

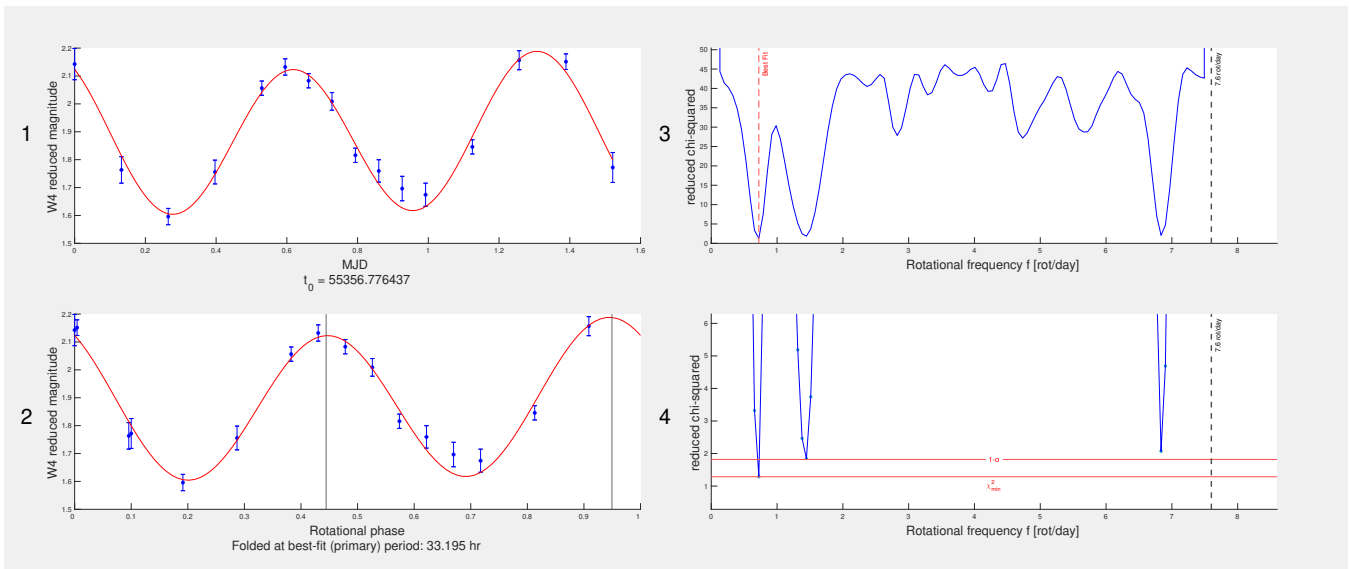


Figure 4. Spin period solution for asteroid 2715 obtained from 16 W4 observations spanning 1.5 days. The period solution at 33.195 ± 2.19 hr is in good agreement with the LCDB value of 33.62 hr. The correct solution was identified despite a data observation span that is only slightly longer than the spin period.

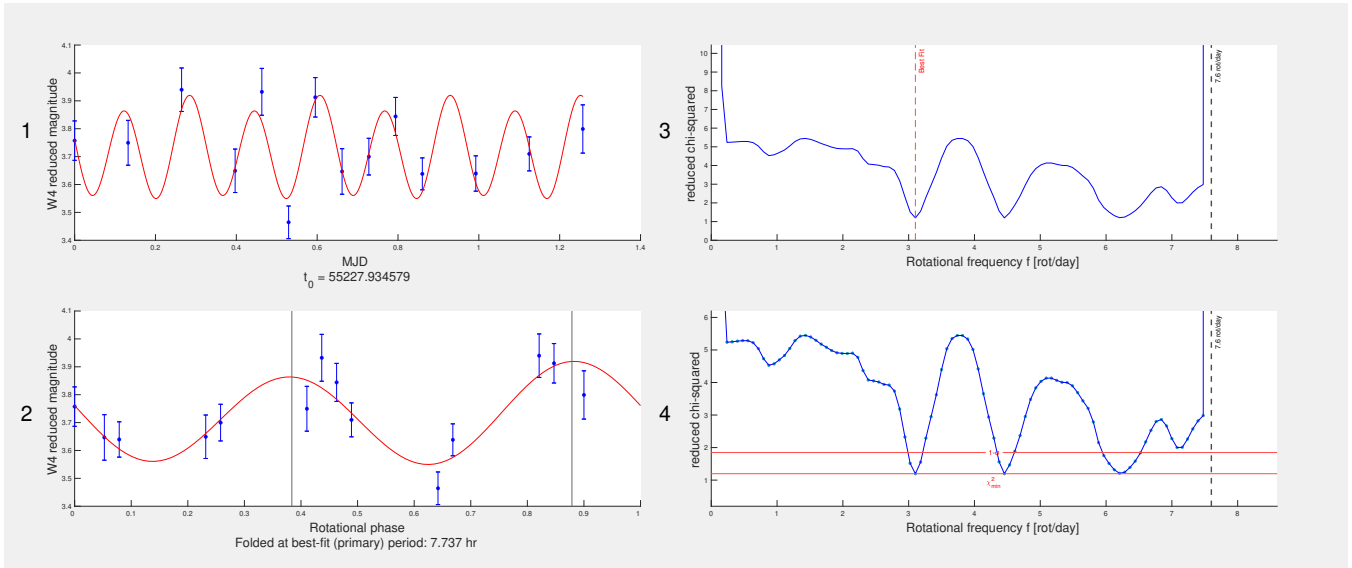


Figure 5. Spin period solution for asteroid 2812 obtained from 14 W4 observations spanning 1.2 days. The period solution at 7.737 ± 0.30 hr is in good agreement with the LCDB value of 7.7 hr. The correct solution was identified despite a relatively low S/N and the presence of competing solutions with similar but larger χ^2 values.

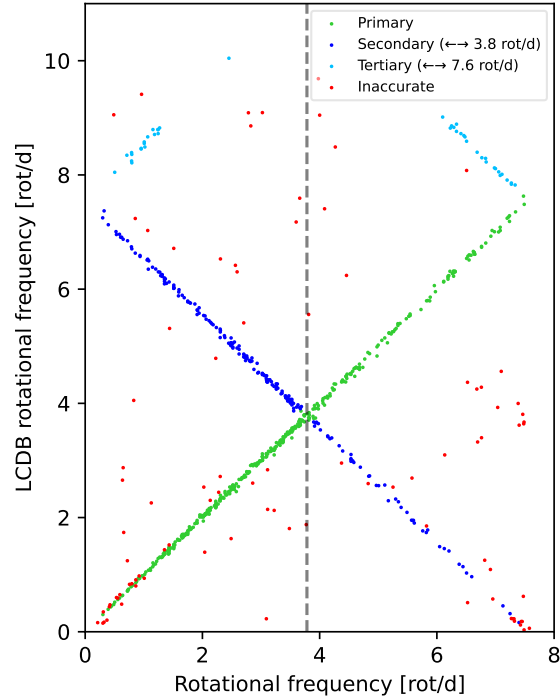


Figure 6. Best-fit rotational frequency (this work) vs. LCDB rotational frequency for the LCDB reference group. The dashed grey line is at $f = 3.7831$ rot/day, which is the expected folding frequency for a 3.17 hr cadence and the predominant aliasing mode. Most of the best-fit solutions (55%) are accurate (green dots). The solutions mirrored about 3.7831 rot/day (dark blue dots) are also accurate in 27% of the cases, and the solutions mirrored about 7.5662 rot/day (light blue dots) are accurate in 6% of the cases. The inaccurate solutions (red dots) represent 12% of the cases. The combination of best-fit and mirrored solutions yields an aggregate success rate of 88%.

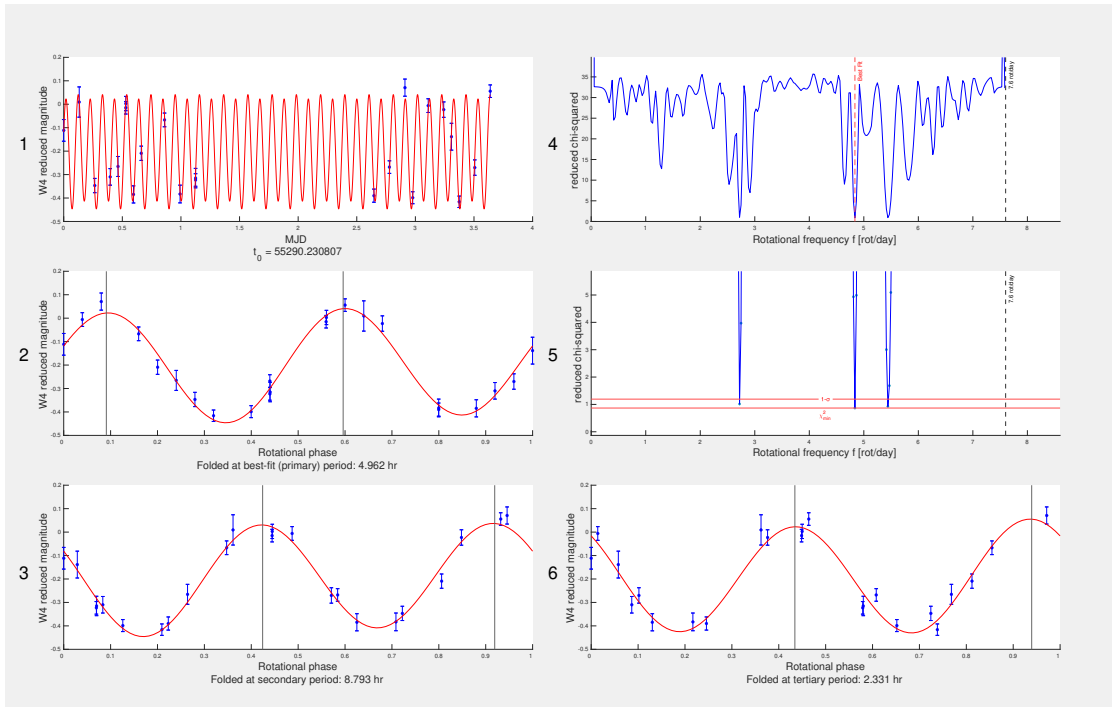


Figure 7. Spin period solution for asteroid 4715 obtained from 23 W4 observations spanning 3.6 days. The best-fit, primary period solution at 4.962 ± 0.01 hr (4.84 rot/day) is an alias (mirrored around $f = 3.7831$ rot/day) of the presumed correct LCDB value of 8.8129 hr (2.72 rot/day). The secondary period solution at 8.7930 hr is accurate at the 0.2% level.

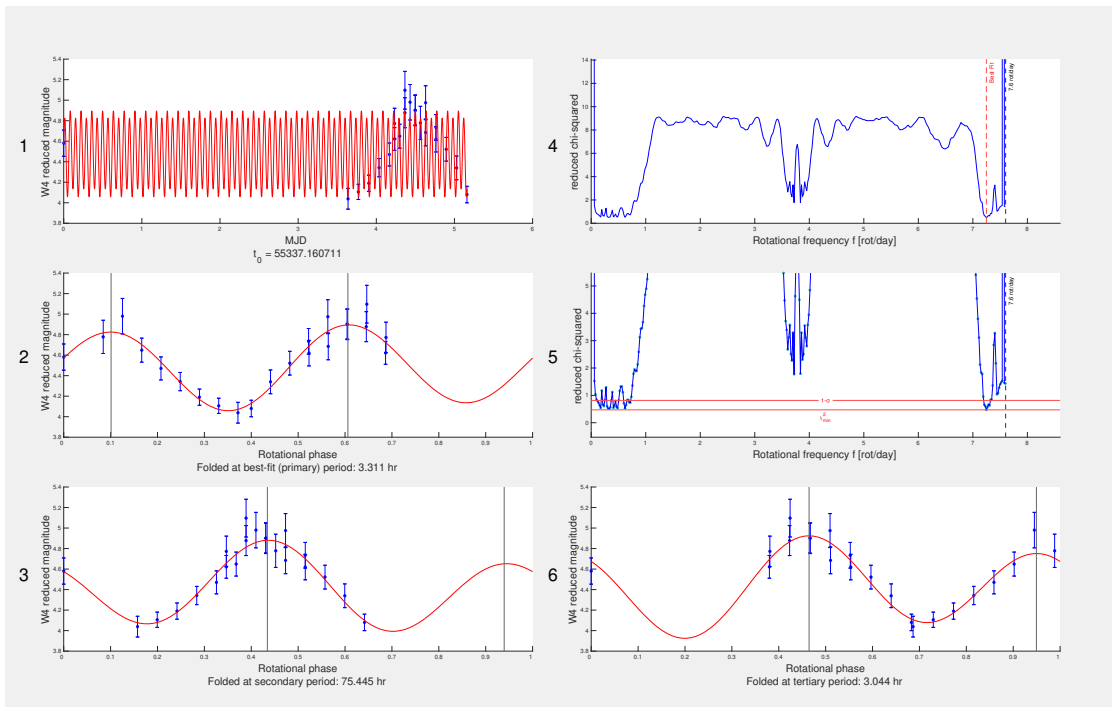


Figure 8. Spin period solution for asteroid 6485 obtained from 22 W4 observations spanning 5.2 days. The best-fit, primary period solution at 3.311 ± 0.035 hr (7.25 rot/day) is an alias (mirrored around $f = 3.7831$ rot/day) of the presumed correct LCDB value of 75.56 hr (0.318 rot/day). The secondary period solution at 75.445 hr is accurate at the 0.2% level.

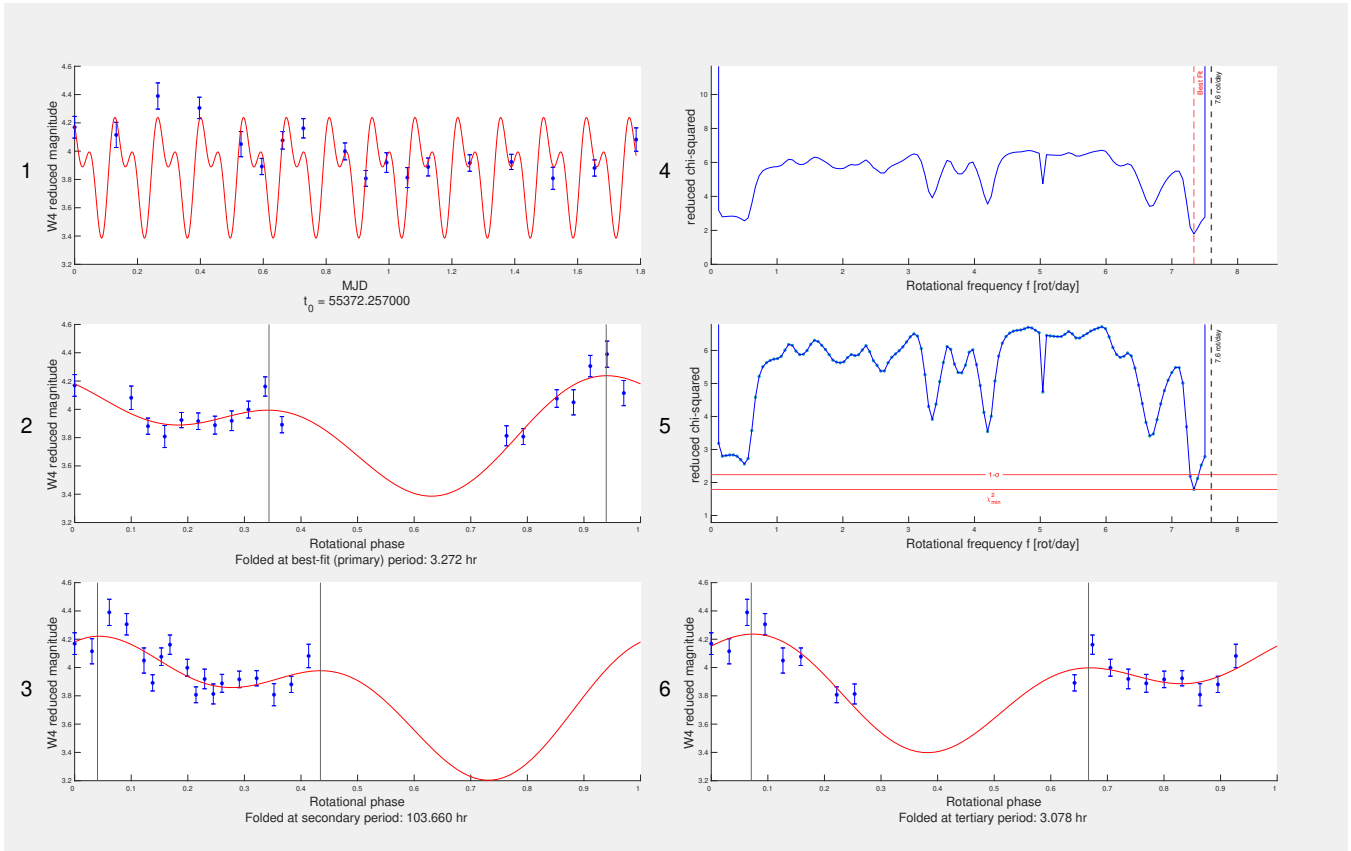


Figure 9. Spin period solution for asteroid 10721 obtained from 18 W4 observations spanning 1.8 days. The period solution at 3.272 ± 0.031 hr (7.33 rot/day) is an alias (mirrored around $f = 7.5662$ rot/day) of the presumed correct LCDB value of 3.0675 hr (7.82 rot/day). The tertiary period solution at 3.078 hr is accurate at the 0.3% level.

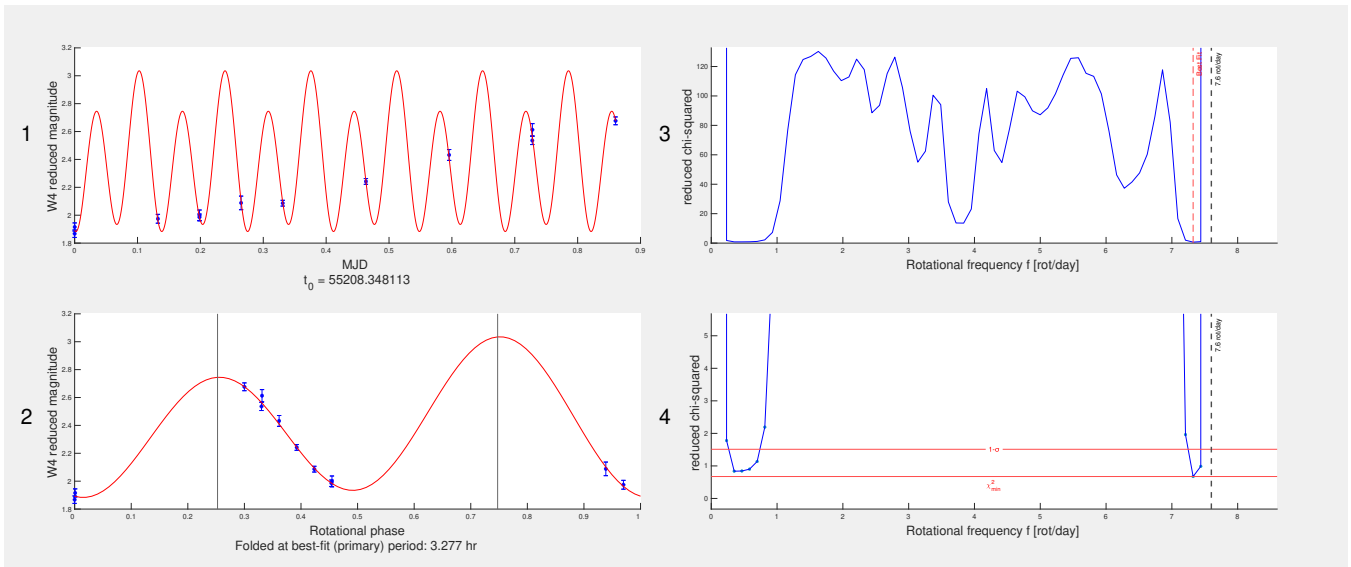


Figure 10. Incorrect spin period solution for asteroid 244 obtained from 12 W4 observations spanning 20.6 hr. None of our solutions match the LCDB period (129.5 hr or 5.4 days). WISE observations of this slow rotator cover only a small fraction of the full rotational phase, which prevents accurate recovery of the spin period.

Table 3. Spin period solutions for 1929 asteroids.

Object	D (km)	span (hr)	idx	A (mag)	P (hr)	σ_P (hr)	f (rot/d)	f_{\leftrightarrow} (rot/d)	P_{\leftrightarrow} (hr)	f_{\leftrightarrow} (rot/d)	P_{\leftrightarrow} (hr)	f_{\leftrightarrow} (rot/d)	P_{\leftrightarrow} (hr)	P_{LCDB} (hr)	A_{min} (mag)	A_{max} (mag)	U	flag
131	30.6	109.5	1	0.358	5.1919	0.019	4.6226	2.9436	8.1532	10.5098	2.2836	5.1812	0.080	0.320	3	1		
155	44.6	93.7	1	0.234	5.2919	0.016	4.5352	3.0310	7.9183	10.5972	2.2648	7.9597	0.110	0.460	3	2		
170	35.4	181.0	1	0.360	13.0199	0.245	1.8433	5.7229	4.1937	9.4095	2.5506	13.1200	0.130	0.300	3	1		
180	24.8	96.9	1	0.493	23.6223	0.486	1.0160	6.5502	3.6640	8.5822	2.7965	23.8660	0.420	0.600	3	1		
183	30.7	90.5	1	0.395	11.7553	0.094	2.0416	5.5246	4.3442	9.6078	2.4980	11.7700	0.200	0.310	3	1		
183	30.8	106.4	2	0.431	11.8183	0.114	2.0308	5.5354	4.3357	9.5970	2.5008	11.7700	0.200	0.310	3	1		
...
244	10.9	20.6	1	1.152	3.2773	0.085	7.3230	0.2432	98.6986	7.8094	3.0732	129.5100	0.800	0.820	3-	0		
296	9.0	141.3	1	0.390	4.5431	0.014	5.2828	2.2834	10.5105	9.8496	2.4366	4.5385	0.380	0.700	3	1		
2715	14.0	36.5	1	0.584	33.1949	2.054	0.7230	6.8432	3.5071	8.2892	2.8953	33.6200	0.540	0.550	3-	1		
2812	6.0	30.2	1	0.370	7.7367	0.290	3.1021	4.4641	5.3762	10.6683	2.2497	7.7000	0.250	0.250	3	1		
4715	71.4	87.3	1	0.487	4.9620	0.010	4.8367	2.7295	8.7930	10.2957	2.3311	8.8129	0.390	0.540	3	2		
6485	3.7	123.8	1	0.837	3.3112	0.035	7.2481	0.3181	75.4453	7.8843	3.0440	75.5600	1.000	1.130	3-	2		
10721	4.7	42.9	1	0.852	3.2721	0.032	7.3347	0.2315	103.6603	7.7977	3.0778	3.0675	0.270	0.270	3	3		
...
256155	3.1	134.9	1	0.550	15.6910	0.118	1.5295	6.0367	3.9757	9.0957	2.6386	
307840	6.8	335.1	1	0.368	16.0317	0.151	1.4970	6.0692	3.9544	9.0632	2.6481	
318081	5.9	42.9	1	0.410	3.6023	0.029	6.6623	0.9039	26.5523	8.4701	2.8335	
366774	0.9	58.8	1	0.327	3.4972	0.036	6.8625	0.7037	34.1075	8.2699	2.9021	
386720	1.0	141.3	1	0.806	4.6034	0.015	5.2136	2.3526	10.2013	9.9188	2.4196	

NOTE—For each object, we show the WISE-derived diameter D (km) (Myhrvold et al. 2022), observation span (hr), index of the cluster of observations analyzed, the best-fit period P (hr), the peak-to-peak magnitude variation of the fitted lightcurve A for the primary (best-fit) period solution, the primary period uncertainty σ_P (hr), the best-fit rotational frequency f (rot/d), the first alternate rotational frequency f_{\leftrightarrow} (rot/d) found by folding the best-fit frequency about 3.7831 rot/day, the first alternate period P_{\leftrightarrow} (hr), the second alternate rotational frequency f_{\leftrightarrow} (rot/d) found by folding the best-fit frequency about 7.5662 rot/day, the second alternate period P_{\leftrightarrow} (hr), the LCDB period P_{LCDB} (hr), the LCDB’s minimum amplitude A_{min} if a range was provided, the LCDB’s amplitude or maximum amplitude A_{max} if a range was provided, the corresponding quality code U , and a flag indicating agreement for objects in the LCDB Reference Group. The flag is 1 if the best-fit period matches P_{LCDB} within 5%, 2 if the first mirror period matches, 3 if the second mirror period matches, and 0 if none of the three periods match P_{LCDB} . Spin period solutions for asteroids shown in Figures 3, 5, 4, 7, 8, 9, and 10 are included. (This table is available in its entirety in [machine-readable](#) and [CSV](#) forms in the online journal. A portion is shown here for guidance regarding its form and content.)

We also validated the amplitudes of our primary lightcurve solutions by comparing them to the amplitudes in the LCDB reference group. For this comparison, we used the arithmetic average of the LCDB’s AMIN and AMAX values when more than one amplitude value was provided in the LCDB. By and large there is good agreement, although our values appear to have an overall bias of approximately 0.1 mag (Figure 11). In the LCDB reference group, 8 out of 752 (1%) solutions have an amplitude that exceeds the LCDB amplitude by 1 mag, and 22 additional solutions (3%) have an amplitude that exceeds the LCDB amplitude by 0.5 mag. We observed that large rotational phase gaps in the timeseries can occasionally result in excessive amplitudes. The worst-case example is asteroid 37152, which happens to have a spin period almost exactly equal to three times the WISE cadence. The second worst-case example is asteroid 4825, which has rotational phase gaps of up to ~ 0.4 . Our best-fit amplitude (2.678 mag) exceeds the LCDB published value (0.705 mag) by ~ 2 mag.

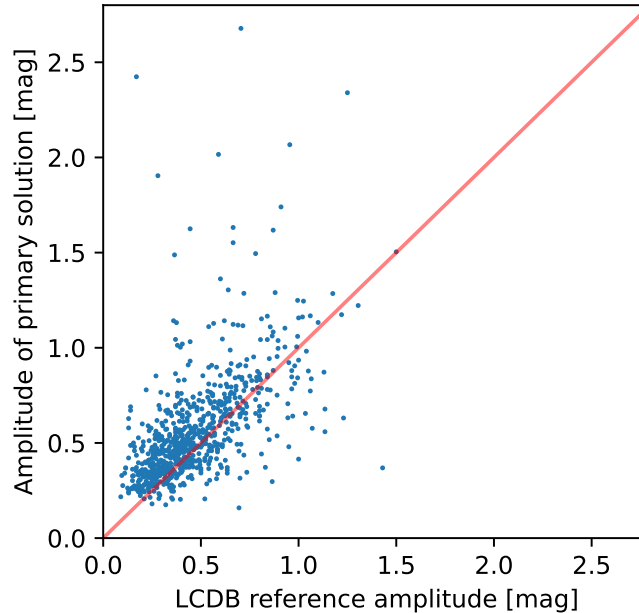


Figure 11. Scatter plot of the lightcurve amplitudes of our primary solutions for the 752 objects in the LCDB reference group and corresponding LCDB amplitudes.

3.2. Lomb-Scargle Pipeline

As in our default pipeline, we generated three candidate period solutions for each fitted lightcurve (primary: LS solution, secondary: mirror across 3.7831 rot/day, tertiary: mirror across 7.5662 rot/day). We compared the accuracy of the LS pipeline to our default pipeline by computing the number of solutions that are within 5% of the high-quality (3/3-) LCDB solutions (Table 4).

Accuracy flag	LS first order	LS second order	Default pipeline
0 (inaccurate)	91 (12%)	518 (52%)	93 (12%)
1 (primary)	320 (43%)	316 (32%)	414 (55%)
2 (secondary)	286 (39%)	105 (11%)	203 (27%)
3 (tertiary)	33 (5%)	56 (6%)	42 (6%)
Aggregate accuracy	88%	48%	88%
Number of reference solutions	730	995	752

Table 4. Number of accurate solutions with the Lomb-Scargle and default pipelines.

The first-order LS solutions have an aggregate accuracy comparable to the default pipeline solutions. However, the primary LS solutions were accurate only in 43% of the cases, compared to 55% in the default pipeline. The second-order LS solutions have a lower accuracy rate than the default pipeline solutions, both for primary solutions and in aggregate. The lower performance of the LS algorithm demonstrates the importance of the iterative algorithm and post-fit filters in our default, Waszczak et al. (2015)-inspired pipeline.

4. DISCUSSION

Pravec et al. (2002) reviewed the rotation periods of asteroids as a function of diameter and found that the spin distribution is Maxwellian for large asteroids (>40 km) and strongly non-Maxwellian for smaller asteroids, with an excess of both slowly rotating and rapidly rotating asteroids. The WISE data set can potentially inform these studies because it can yield estimates of both diameter and spin period (Figure 12). However, the value of our estimates in this context is diminished because of obvious selection effects with respect to spin period.

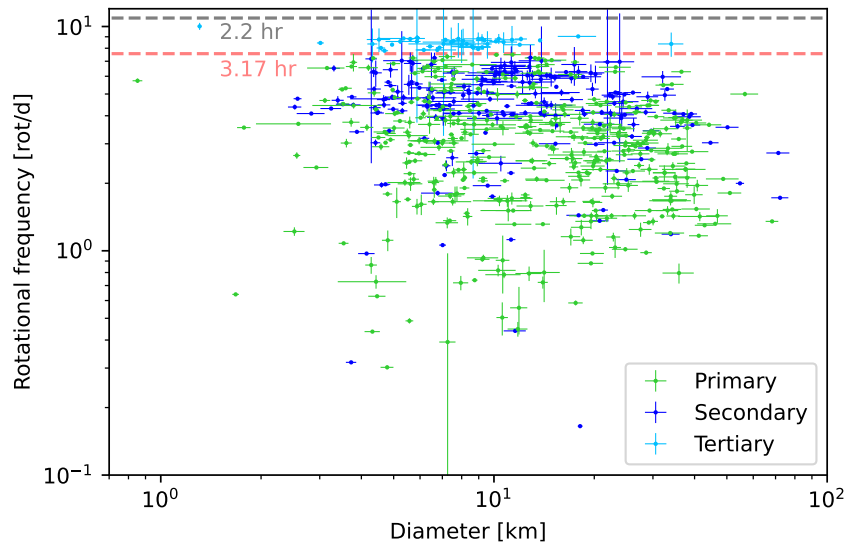


Figure 12. Rotational frequency vs. diameter diagram for the 659 light curves in the LCDB reference group where one of our spin period solutions matched the LCDB to 5%. Only the spin period solutions that match the LCDB value are plotted, with color-coding indicating our primary, secondary, or tertiary solutions. The red dashed line at $P = 3.17$ hr corresponds to the upper range of trial frequencies explored in the fitting process. The grey dashed line at $P = 2.2$ hr illustrates the spin barrier. Diameters are from Myhrvold et al. (2022).

We can evaluate the accuracy of our method as function of asteroid diameter and LCDB period (Figure 13). Diameter does not have an apparent influence on the accuracy of our method. However, spin period does affect our ability to recover a correct solution with the WISE data. We found that the spin periods of both slowly rotating ($P > \sim 100$ hr) and rapidly rotating ($P < \sim 2.5$ hr) asteroids are generally not recoverable.

The distribution of lightcurve amplitudes in our data set is instructive (Figure 14). Our distribution underestimates the proportion of low-amplitude lightcurves, because our sample selection enforced a pre-fit filter, which required a magnitude variation of at least 0.3 mag in the observed fluxes. The bias against low-amplitude lightcurves is not limited to our work. Likewise, one of our post-fit filters eliminated some high-amplitude lightcurve solutions, but it did so only when the data themselves did not exhibit a large magnitude variation. We found that 50%, 8.8%, 2.2%, 1%, and 0.25% of solutions have amplitudes larger than 0.5 mag, 1 mag, 1.5 mag, 2 mag, and 2.5 mag, respectively.

Aliasing in our solutions was exacerbated by the quasi-uniform cadence of WISE observations. Although recovery from aliasing is relatively straightforward, it is possible to reduce the presence of aliased solutions with non-uniform sampling. To illustrate this point, we generated 100 sequences of simulated observations of asteroid 4715 (Figure 7) with \sim uniform (WISE) sampling and 100 sequences with non-uniform sampling, all with the same number of observations over the same time interval. All simulated observations were generated with a sixth-order Fourier series and polluted

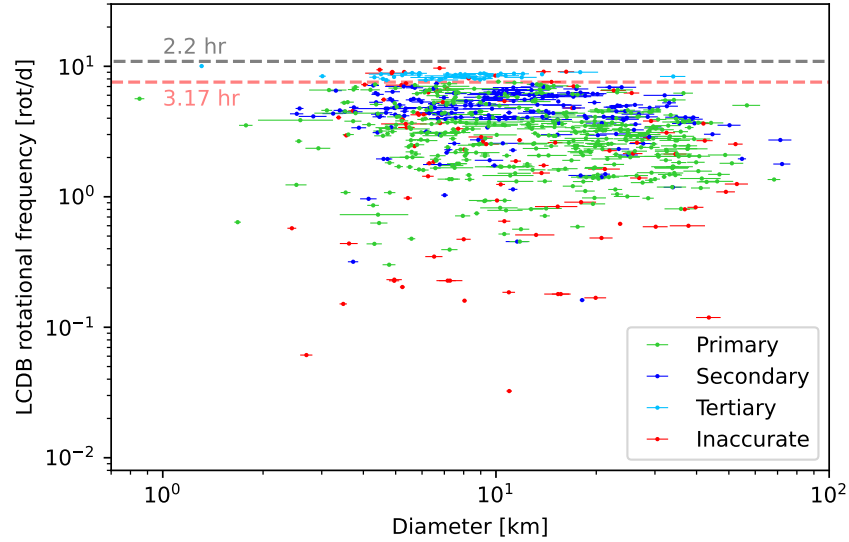


Figure 13. LCDB rotational frequency vs. diameter (Myhrvold et al. 2022) for the 752 lightcurves in the LCDB Reference Group. Our spin period solutions are color-coded according to four possible outcomes: primary solution is accurate, secondary solution is accurate, tertiary solution is accurate, or none are accurate. The red dashed line at $P = 3.17$ hr corresponds to the upper range of trial frequencies explored in the fitting process. The grey dashed line at $P = 2.2$ hr illustrates the spin barrier. Diameters are from Myhrvold et al. (2022).

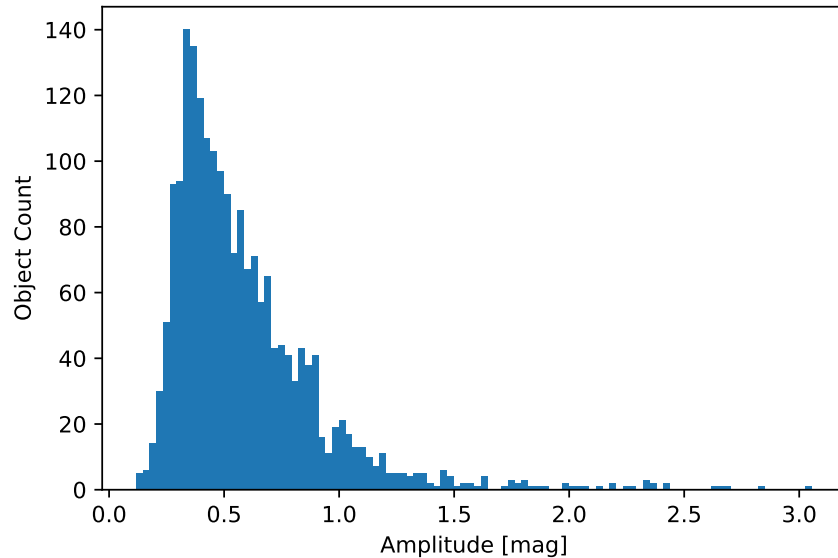


Figure 14. Histogram of peak-to-peak lightcurve amplitudes.

with random Gaussian noise ($\sigma=0.05$ mag). Among the 100 uniformly sampled sequences, 89 yielded the correct solution and 11 yielded a (recoverable) aliased solution mirrored around the $f = 3.7831$ rot/day axis. All non-uniformly sampled solutions yielded the correct solution. For this reason, ground-based observers may wish to intentionally deviate from a strictly regular cadence.

5. CONCLUSIONS

We devised a procedure similar to that of [Waszczak et al. \(2015\)](#) that enables the determination of thousands of asteroid spin periods from WISE data. Despite WISE’s suboptimal observation and cadence for asteroid spin measurements, one of our solutions is accurate 88% of the time when compared to a high-quality control group of 752 spin periods. We obtained primary, secondary, and tertiary spin period estimates for 2008 observation clusters representing 1929 unique asteroids. Among those, 1205 asteroids do not currently have a high-quality spin period estimate. Our primary, secondary, or tertiary solutions for over a thousand asteroids are expected to be accurate at the 5% level or better and can greatly facilitate shape or thermal modeling work. In addition, they may reveal objects with unusual lightcurves worthy of more thorough observations.

ACKNOWLEDGMENTS

We thank Alan Harris (California) and an anonymous reviewer for insightful and constructive reviews. We thank Robert D. Stephens for providing Fourier coefficients for the lightcurve of 4715. A.L. was funded in part by the Joe and Andrea Straus Endowment for Undergrad Opportunity and the Donald Carlisle Undergrad Research Endowed Fund. E.W. was funded in part by the Nathan P. Myhrvold Graduate Fellowship. A.L. thanks Breann Sitarski for her helpful feedback on this work and the related research presentations, as well as her mentorship throughout his undergraduate studies. This publication makes use of data products from the Wide-field Infrared Survey Explorer, which is a joint project of the University of California, Los Angeles, and the Jet Propulsion Laboratory/California Institute of Technology, funded by the National Aeronautics and Space Administration.

Software: NumPy ([Harris et al. 2020](#)), SciPy ([Virtanen et al. 2020](#)), pandas ([Wes McKinney 2010](#)), Matplotlib ([Hunter 2007](#))

APPENDIX

A. ALIASING

The observation cadence, i.e., the series of time intervals between consecutive photometric measurements, is an important factor in the analysis of asteroid spin periods. If the sampling does not yield at least two points per cycle, aliasing occurs. Aliasing often produces replicas of the peak corresponding to the correct period in the power spectrum, precluding a unique period determination. These peaks may exhibit some asymmetry in the misfit values displayed in the periodogram, and the correct period is not guaranteed to have the best-fit value. In the case of asteroid spin determinations from WISE, the problems associated with aliasing and asymmetry are amplified because of the sparsity of data points, short observation spans, and measurement noise.

We expect signals with frequencies > 7.5662 rot/day to alias and fold about the 7.5662 rot/day axis. We also expect folding about the 3.7831 rot/day axis due to presence of sampling intervals at 3.17 hr. While some mirroring behavior is obvious, it is not always possible to detect which axis was involved in the folding behavior. We took several actions to maximize the reliability in the recovered period solutions.

First, we limited the range of scanned frequencies to the Nyquist rate corresponding to the 1.59 hr cadence (Section 2.3). A drawback of this approach is that it initially prevents recovery of the spin periods of asteroids that rotate faster than $f = 7.5662$ rot/day, which amount to approximately 17% of asteroids in our sample. However, a fraction of these solutions are recovered because we provide the solution that is mirrored about the $f = 7.5662$ rot/day axis.

Second, we eliminated time series where the minimum cadence is 3.17 hr or above (Section 2.2.4) because these data are most prone to aliasing. For the same reason, we preferred the W4 data over the W3 data (Section 2.2.3).

Third, we attempted to reject aliased solutions based on domain knowledge. We required double-peaked folded lightcurves with a peak ratio of two or larger (Section 2.3) to encourage a second-order dominant Fourier series.

REFERENCES

- | | |
|---|---|
| <p>Benner, L. A. M., Busch, M. W., Giorgini, J. D., Taylor, P. A., & Margot, J. L. 2015, in <i>Asteroids IV</i>, ed. P. Michel, F. E. DeMeo, & W. F. Bottke (Univ. of Arizona Press), 165–182, doi: 10.2458/azu_uapress_9780816530595-ch009</p> | <p>Bottke, W. F., Brož, M., O’Brien, D. P., et al. 2015, in <i>Asteroids IV</i>, ed. P. Michel, F. E. DeMeo, & W. F. Bottke (Univ. of Arizona Press), 701–724, doi: 10.2458/azu_uapress_9780816532131-ch036</p> |
|---|---|

- Chang, C.-K., Lin, H.-W., Ip, W.-H., et al. 2017, *Geoscience Letters*, 4, 17, doi: [10.1186/s40562-017-0082-7](https://doi.org/10.1186/s40562-017-0082-7)
- Cutri, R., Sonnett, S., Masiero, J., et al. 2019, in EPSC-DPS Joint Meeting 2019, Vol. 2019, EPSC-DPS2019-1012
- Delbo, M., Mueller, M., Emery, J. P., Rozitis, B., & Capria, M. T. 2015, in *Asteroids IV*, ed. P. Michel, F. E. DeMeo, & W. F. Bottke (Univ. of Arizona Press), 107–128, doi: [10.2458/azu_uapress.9780816532131-ch006](https://doi.org/10.2458/azu_uapress.9780816532131-ch006)
- Durech, J., Carry, B., Delbo, M., Kaasalainen, M., & Viikinkoski, M. 2015, in *Asteroids IV*, ed. P. Michel, F. E. DeMeo, & W. F. Bottke (Univ. of Arizona Press), 183–202, doi: [10.2458/azu_uapress.9780816532131-ch010](https://doi.org/10.2458/azu_uapress.9780816532131-ch010)
- Ďurech, J., Hanuš, J., & Alí-Lagoa, V. 2018, *Astronomy & Astrophysics*, 617, A57, doi: [10.1051/0004-6361/201833437](https://doi.org/10.1051/0004-6361/201833437)
- Ďurech, J., et al. 2015, *Proceedings of the International Astronomical Union*, 10, 170, doi: [10.1017/s1743921315008492](https://doi.org/10.1017/s1743921315008492)
- Greenberg, A. H., Margot, J.-L., Verma, A. K., Taylor, P. A., & Hodge, S. E. 2020, *Astron. J.*, 159, 92, doi: [10.3847/1538-3881/ab62a3](https://doi.org/10.3847/1538-3881/ab62a3)
- Hanuš, J., Delbo, M., Ďurech, J., & Alí-Lagoa, V. 2015, *Icarus*, 256, 101, doi: [10.1016/j.icarus.2015.04.014](https://doi.org/10.1016/j.icarus.2015.04.014)
- Harris, A., Pravec, P., Galád, A., et al. 2014, *Icarus*, 235, 55, doi: <https://doi.org/10.1016/j.icarus.2014.03.004>
- Harris, A. W., Pravec, P., & Warner, B. D. 2012, *Icarus*, 221, 226, doi: [10.1016/j.icarus.2012.06.046](https://doi.org/10.1016/j.icarus.2012.06.046)
- Harris, A. W., Young, J. W., Bowell, E., et al. 1989, *Icarus*, 77, 171, doi: [10.1016/0019-1035\(89\)90015-8](https://doi.org/10.1016/0019-1035(89)90015-8)
- Harris, C. R., Millman, K. J., van der Walt, S. J., et al. 2020, *Nature*, 585, 357–362, doi: [10.1038/s41586-020-2649-2](https://doi.org/10.1038/s41586-020-2649-2)
- Hora, J. L., Siraj, A., Mommert, M., et al. 2018, *The Astrophysical Journal Supplement Series*, 238, 22, doi: [10.3847/1538-4365/aadcf5](https://doi.org/10.3847/1538-4365/aadcf5)
- Hunter, J. D. 2007, *Computing in Science Engineering*, 9, 90, doi: [10.1109/MCSE.2007.55](https://doi.org/10.1109/MCSE.2007.55)
- Lomb, N. R. 1976, *Ap&SS*, 39, 447, doi: [10.1007/BF00648343](https://doi.org/10.1007/BF00648343)
- Mainzer, A., Usui, F., & Trilling, D. E. 2015, in *Asteroids IV*, ed. P. Michel, F. E. DeMeo, & W. F. Bottke (Univ. of Arizona Press), 89–106, doi: [10.2458/azu_uapress.9780816532131-ch005](https://doi.org/10.2458/azu_uapress.9780816532131-ch005)
- Margot, J.-L., Pinchuk, P., & Myhrvold, N. 2023, Data from: Analysis of four-band WISE observations of asteroids, Dryad, doi: [10.5068/D10D6G](https://doi.org/10.5068/D10D6G)
- Margot, J. L., Pravec, P., Taylor, P., Carry, B., & Jacobson, S. 2015, in *Asteroids IV*, ed. P. Michel, F. E. DeMeo, & W. F. Bottke (Univ. of Arizona Press), 355–373, doi: [10.2458/azu_uapress.9780816532131-ch019](https://doi.org/10.2458/azu_uapress.9780816532131-ch019)
- McNeill, A., Mommert, M., Trilling, D. E., Llama, J., & Skiff, B. 2019, *ApJS*, 245, 29, doi: [10.3847/1538-4365/ab5223](https://doi.org/10.3847/1538-4365/ab5223)
- Muononen, K., Belskaya, I. N., Cellino, A., et al. 2010, *Icarus*, 209, 542, doi: [10.1016/j.icarus.2010.04.003](https://doi.org/10.1016/j.icarus.2010.04.003)
- Myhrvold, N. 2018, *Icarus*, 314, 64, doi: [10.1016/j.icarus.2018.05.004](https://doi.org/10.1016/j.icarus.2018.05.004)
- Myhrvold, N., Pinchuk, P., & Margot, J.-L. 2022, *Planetary Science Journal*, 3, 30, doi: [10.3847/PSJ/ac3232](https://doi.org/10.3847/PSJ/ac3232)
- Naidu, S. P., Margot, J. L., Taylor, P. A., et al. 2015, *AJ*, 150, 54, doi: [10.1088/0004-6256/150/2/54](https://doi.org/10.1088/0004-6256/150/2/54)
- Ostro, S. J., Hudson, R. S., Benner, L. A. M., et al. 2002, in *Asteroids III*, ed. W. F. Bottke, A. Cellino, P. Paolicchi, & R. P. Binzel (Univ. of Arizona Press), 151–168
- Ostro, S. J., Margot, J. L., Benner, L. A. M., et al. 2006, *Science*, 314, 1276, doi: [10.1126/science.1133622](https://doi.org/10.1126/science.1133622)
- Pravec, P., Harris, A. W., & Michalowski, M. 2002, in *Asteroids III*, ed. W. F. Bottke, A. Cellino, P. Paolicchi, & R. P. Binzel (Univ. of Arizona Press), 113–122
- Press, W. H., Teukolsky, S. A., Vetterling, W. T., & Flannery, B. P. 1992, *Numerical Recipes in C - The Art of Scientific Computing*, 2nd edn. (Cambridge: Cambridge University Press)
- Scargle, J. D. 1982, *ApJ*, 263, 835, doi: [10.1086/160554](https://doi.org/10.1086/160554)
- Scheeres, D. J., Britt, D., Carry, B., & Holsapple, K. A. 2015, in *Asteroids IV*, ed. P. Michel, F. E. DeMeo, & W. F. Bottke (Univ. of Arizona Press), 745–766, doi: [10.2458/azu_uapress.9780816532131-ch038](https://doi.org/10.2458/azu_uapress.9780816532131-ch038)
- Virtanen, P., Gommers, R., Oliphant, T. E., et al. 2020, *Nature Methods*, 17, 261, doi: <https://doi.org/10.1038/s41592-019-0686-2>
- Vokrouhlický, D., Bottke, W. F., Chesley, S. R., Scheeres, D. J., & Statler, T. S. 2015, in *Asteroids IV*, ed. P. Michel, F. E. DeMeo, & W. F. Bottke (Univ. of Arizona Press), 509–531, doi: [10.2458/azu_uapress.9780816532131-ch027](https://doi.org/10.2458/azu_uapress.9780816532131-ch027)
- Walsh, K. J., & Jacobson, S. A. 2015, in *Asteroids IV*, ed. P. Michel, F. E. DeMeo, & W. F. Bottke (Univ. of Arizona Press), 375–393, doi: [10.2458/azu_uapress.9780816532131-ch020](https://doi.org/10.2458/azu_uapress.9780816532131-ch020)
- Warner, B.D. and Harris, A.W. and Pravec, P. 2021, Asteroid Lightcurve Data Base (LCDB) Bundle V4.0., NASA Planetary Data System, doi: [10.26033/j3xc-3359](https://doi.org/10.26033/j3xc-3359)
- Waszczak, A., Chang, C.-K., Ofek, E. O., et al. 2015, *AJ*, 150, 75, doi: [10.1088/0004-6256/150/3/75](https://doi.org/10.1088/0004-6256/150/3/75)

Wes McKinney. 2010, in Proceedings of the 9th Python in Science Conference, ed. Stéfan van der Walt & Jarrod Millman, 56 – 61, doi: [10.25080/Majora-92bf1922-00a](https://doi.org/10.25080/Majora-92bf1922-00a)
WISE Team. 2020, WISE All-Sky Single Exposure (L1b) Source Table, Dataset, IPAC, doi: [10.26131/IRSA139](https://doi.org/10.26131/IRSA139)

Wright, E. L., Eisenhardt, P. R. M., Mainzer, A. K., et al. 2010, AJ, 140, 1868, doi: [10.1088/0004-6256/140/6/1868](https://doi.org/10.1088/0004-6256/140/6/1868)
Zechmeister, M., & Kürster, M. 2009, A&A, 496, 577, doi: [10.1051/0004-6361:200811296](https://doi.org/10.1051/0004-6361:200811296)